Computer Methods in Applied Mechanics and Engineering 107 (1993) 269–298
North-Holland

CMA 400

A finite element formulation for the hydrodynamic semiconductor device equations

N.R. Aluru[a], A. Raefsky[b], P.M. Pinsky[a], K.H. Law[a], R.J.G. Goossens[b] and R.W. Dutton[b]

[a]*Department of Civil Engineering, Stanford University, Stanford, CA 94305, USA*
[b]*Department of Electrical Engineering, Stanford University, Stanford, CA 94305, USA*

Received 21 September 1992

A new formulation employing the Galerkin/least-squares finite element method is presented for the simulation of the hydrodynamic model of semiconductor devices. Numerical simulations are performed on the coupled Poisson and hydrodynamic equations for one carrier devices. The hydrodynamic equations for a single carrier, i.e. for the electrons or holes, resemble the compressible Navier–Stokes equations with the addition of highly nonlinear source terms and without the viscous terms. The governing equations are nondimensionalized to improve the conditioning on the resulting system of equations and the efficiency of the numerical algorithms. Furthermore, to establish the stability of the discrete solution, the system of hydrodynamic equations is symmetrized by considering generalized entropy functions. A staggered solution strategy is employed to treat the coupled hydrodynamic and Poisson equations. Numerical results are presented for one-dimensional and two-dimensional one-carrier n^+-n-n^+ devices. The presence of velocity overshoot has been observed and it is recognized that the heat flux term plays an important role in the simulation of semiconductor devices employing the hydrodynamic model.

1. Introduction

The simulation of the electrical characteristics of semiconductor devices has been an active area of research for over a decade. Such research has led to the development of a series of increasingly powerful and full-featured simulators [1]. Recent advancements in three distinct areas have created the opportunity for another round of breakthrough developments.

Firstly, continued device miniaturization has pushed geometry sizes down to below 0.5 μm, leading to ever higher electrical fields. Therefore, it is no longer reasonable to assume a simple linear relationship between carrier velocity and local electric field. Instead, more complicated models are needed to explicitly deal with this carrier-heating phenomenon. As a result, there has been a shift away from the commonly used drift-diffusion model. The two main contenders are the energy-transport [2] and the hydrodynamic model [3–7]. The latter set of equations obtains its name from the strong similarity to the compressible Euler and Navier–Stokes equations governing fluid flow. Current simulators dealing with the hydrodynamic

Correspondence to: Professor Kincho Law, Stanford University, Department of Civil Engineering, Terman Engineering Center, Room 242, Stanford, CA 94305, USA.

(HD) model have been rather restricted: many only deal with 1-D problems, all rely on ad-hoc heuristic numerical 'tricks' to help the solution process, none have systematically dealt with verification of correctness.

Secondly, in the area of computational fluid dynamics, developments over the past 5 years in the Galerkin/least-squares finite element formulation of compressible Euler and Navier–Stokes equations have led to very general, robust, and accurate codes [8–10, 15, 19, 21, 22]. To our knowledge, there is no literature employing these methods to the hydrodynamic model for the semiconductor device equations.

Thirdly, implementations of the Galerkin/least-squares finite element method map nicely onto modern massively parallel architectures as has been demonstrated through the solution of million-element problems on highly unstructured grids [11]. This has made it possible to attack interesting engineering problems with a realistic degree of complexity and produce solutions within a reasonable time.

In this paper, we propose a space-time Galerkin/least-squares finite element method based on the hydrodynamic model for semiconductor devices. Coupled hydrodynamic and Poisson equations are solved using a staggered scheme. The non-symmetric, nonlinear hydrodynamic equations are symmetrized with generalized entropy functions. This formulation based on entropy variables automatically satisfies the Clausius–Duhem inequality, or the second law of thermodynamics, which is a basic nonlinear stability requirement. To improve the conditioning of the resulting system of equations, the governing equations are nondimensionalized.

The paper is organized as follows. In Section 2, we review the partial differential equations for the hydrodynamic model and the Poisson equation, establish similarity between the HD equations and the compressible Euler equations, and discuss nondimensionalization procedures. In Section 3, we give the conservation form and present the symmetrization procedure. Section 4 discusses the finitc element formulation of the electron hydrodynamic equations and the Poisson equation. Section 5 discusses the staggered approach that we use to solve the coupled equations. In Section 6, we present the numerical results for one-carrier devices to demonstrate the robustness and applicability of finite element methods for device simulations. In Section 7, we summarize the contributions of this study and future research.

2. Partial differential equations for semiconductor devices

Semiconductor devices can be simulated by solving a set of conservation equations for the electrons and holes coupling with the Poisson equation for the electrostatic potential. The partial differential equations for the conservation laws of electrons and holes are derived from zero-, first-, and second-order moments of Boltzmann's equations [4, 12]. In this section, we review the HD and the Poisson equations. The transport equations for electrons are given as follows:

$$\frac{\partial n}{\partial t} + \nabla\cdot(n\boldsymbol{u}_e) = \left[\frac{\partial n}{\partial t}\right]_{\text{col}}, \tag{1}$$

$$\frac{\partial \boldsymbol{p}_e}{\partial t} + \boldsymbol{u}_e(\nabla\cdot\boldsymbol{p}_e) + (\boldsymbol{p}_e\cdot\nabla)\boldsymbol{u}_e = -\varepsilon n\boldsymbol{E} - \nabla(nk_bT_e) + \left[\frac{\partial \boldsymbol{p}_e}{\partial t}\right]_{\text{col}}, \tag{2}$$

$$\frac{\partial w_e}{\partial t} + \nabla\cdot(\boldsymbol{u}_e w_e) = -\varepsilon n(\boldsymbol{u}_e\cdot\boldsymbol{E}) - \nabla\cdot(\boldsymbol{u}_e n k_b T_e) - \nabla\cdot\boldsymbol{q}_e + \left[\frac{\partial w_e}{\partial t}\right]_{col}. \tag{3}$$

Equations (1), (2) and (3) are the continuity equation and conservation laws for momentum and energy, respectively. A similar set of equations can be derived for holes:

$$\frac{\partial p}{\partial t} + \nabla\cdot(p\boldsymbol{u}_h) = \left[\frac{\partial p}{\partial t}\right]_{col}, \tag{4}$$

$$\frac{\partial \boldsymbol{p}_h}{\partial t} + \boldsymbol{u}_h(\nabla\cdot\boldsymbol{p}_h) + (\boldsymbol{p}_h\cdot\nabla)\boldsymbol{u}_h = \varepsilon p\boldsymbol{E} - \nabla(pk_bT_h) + \left[\frac{\partial \boldsymbol{p}_h}{\partial t}\right]_{col}, \tag{5}$$

$$\frac{\partial w_h}{\partial t} + \nabla\cdot(\boldsymbol{u}_h w_h) = \varepsilon p(\boldsymbol{u}_h\cdot\boldsymbol{E}) - \nabla\cdot(\boldsymbol{u}_h pk_bT_h) - \nabla\cdot\boldsymbol{q}_h + \left[\frac{\partial w_h}{\partial t}\right]_{col}. \tag{6}$$

The electron and hole concentrations are coupled to the electrostatic potential by the Poisson equation. The Poisson equation, derived from Maxwells equations [1, 13], is given by

$$\nabla\cdot(\theta\boldsymbol{E}) = \varepsilon(n - p - N_D^+ + N_A^-), \tag{7}$$

where the electric field $\boldsymbol{E}$ is related to the electrostatic potential ψ by

$$\boldsymbol{E} = -\nabla\psi. \tag{8}$$

In (1)–(7), n and p are the concentration of electrons and holes; $\boldsymbol{u}_e$ and $\boldsymbol{u}_h$ are the electron and hole-velocity vectors; $\boldsymbol{p}_e$ and $\boldsymbol{p}_h$ are the electron and hole momentum density vectors; T_e and T_h are the electron and hole temperatures; w_e and w_h are the electron and hole energy densities; $\boldsymbol{q}_e$ and $\boldsymbol{q}_h$ are the electron and hole heat flux vectors; ε is the magnitude of an elementary charge; k_b is the Boltzmann constant; N_D^+ is the concentration of ionized donor and N_A^- the concentration of ionized acceptor; θ is the dielectric permittivity; $[\,]_{col}$ denotes collision terms. Explicit form of collision terms for one-carrier devices are given in Section 2.3. In the above equations, vectors are denoted by bold letters.

The electron and hole conservation laws are coupled to the Poisson equation through the electric field term appearing on the right-hand side of the equations. Similarly, the Poisson equation is coupled to the electron and hole conservation laws through the concentrations of electrons and holes, which again appear on the right-hand side of the equation. This type of coupling can be considered 'weak' since the coupling terms act primarily as source terms. Due to the nonlinearity of the system, weak interaction between Poisson and hydrodynamic equations does not necessarily imply that the influence of the coupling on the solution is small. We discuss this issue of weak coupling and the solution strategy in more detail in Section 5.

Since the HD equations of electrons and holes are similar, the numerical treatment of the two systems is identical. In this paper, we focus on the formulation for the electron system. For clarity of presentation, the subscript e is removed in the sequel, it being understood that all variables missing a subscript pertain to the electron system.

The electron momentum and energy density can be written as

$$\boldsymbol{p} = mn\boldsymbol{u}, \tag{9}$$

$$w = \frac{3}{2} n k_b T + \frac{1}{2} mn|u|^2 , \tag{10}$$

respectively, where m is the electron mass. The Fourier law for heat conduction is given by

$$q = -\kappa n \nabla T , \tag{11}$$

where

$$\kappa = \frac{3\mu_{n0} k_b^2 T_0}{2\varepsilon} \tag{12}$$

and where μ_{n0} is the electron mobility, and T_0 is the temperature of the lattice.

With appropriate modifications, the HD equations can be written to resemble the equations of compressible gas flow. More specifically, they take the form of Euler equations with $\gamma = 5/3$, for a gas of charged particles in an electric field with the addition of a heat conduction term. The momentum and energy conservation laws, noted in (2) and (3), respectively, can be simplified as shown in the following subsections.

2.1. *Equation for conservation of momentum*

Using indicial notation, equation (2) for the conservation of momentum, can be rewritten as

$$\frac{\partial}{\partial t}(mnu_i) + u_i(mnu_j)_{,j} + mnu_j(u_{i,j}) = -\varepsilon n E_i - (nk_b T)_{,i} + \left[\frac{\partial p_i}{\partial t}\right]_{\text{col}} , \tag{13}$$

where u_i, E_i and $[\partial p_i / \partial t]_{\text{col}}$ denote components of velocity, electric field, and collision terms. Repeated indices implies summation over a range of 1 to 3, and $(\cdot)_{,j}$ denotes differentiation with respect to the jth spatial coordinate. Dividing (13) by the electron mass m and simplifying, we obtain

$$\frac{\partial}{\partial t}(nu_i) + (nu_i u_j)_{,j} = -\frac{\varepsilon}{m} n E_i - \left(\frac{nk_b T}{m}\right)_{,i} + \frac{1}{m}\left[\frac{\partial p_i}{\partial t}\right]_{\text{col}} . \tag{14}$$

If we introduce the *electron pressure* per unit mass, defined as

$$P = \frac{nk_b T}{m} , \tag{15}$$

the momentum equation (14) can be written as

$$\frac{\partial}{\partial t}(nu_i) + (nu_i u_j + P\delta_{ij})_{,j} = -\frac{\varepsilon}{m} n E_i + \frac{1}{m}\left[\frac{\partial p_i}{\partial t}\right]_{\text{col}} , \tag{16}$$

where δ_{ij} is the Kronecker delta. Equation (16) is analogous to the Euler equation for conservation of momentum with the driving forces given in terms of the electric field and collision terms. The definition of electron pressure per unit mass arises naturally from this transformation procedure.

2.2. Equation for conservation of energy

Equation (3) for the conservation of energy can also be rewritten with indicial notation as follows:

$$\frac{\partial w}{\partial t} + (u_i w)_{,i} = -\varepsilon n u_i E_i - (u_i n k_b T)_{,i} - q_{i,i} + \left[\frac{\partial w}{\partial t}\right]_{\text{col}} . \tag{17}$$

Introducing the term *energy density*, defined by

$$w = n m e_{\text{tot}} , \tag{18}$$

where e_{tot} denotes the total energy per unit mass, it follows that

$$e_{\text{tot}} = \frac{3}{2m} k_b T + \frac{1}{2} |u|^2 . \tag{19}$$

It is also useful to introduce the *electron internal energy* per unit mass defined as

$$e_{\text{int}} = \frac{3}{2m} k_b T . \tag{20}$$

The total energy per unit mass of an electron can be written as the sum of the internal energy and kinetic energy per unit mass, i.e.,

$$e_{\text{tot}} = e_{\text{int}} + \tfrac{1}{2}|u|^2 . \tag{21}$$

Using the above equations, the energy conservation equation (17) can be rewritten as

$$\frac{\partial}{\partial t}(n m e_{\text{tot}}) + (n m e_{\text{tot}} u_i + u_i n k_b T)_{,i} = -\varepsilon n u_i E_i - q_{i,i} + \left[\frac{\partial w}{\partial t}\right]_{\text{col}} . \tag{22}$$

Substituting into (22) the electron pressure per unit mass, P, as defined in (15), we obtain

$$\frac{\partial}{\partial t}(n e_{\text{tot}}) + (n e_{\text{tot}} u_i + P u_i)_{,i} = -\frac{\varepsilon n u_i E_i}{m} - q_{i,i} + \frac{1}{m}\left[\frac{\partial w}{\partial t}\right]_{\text{col}} , \tag{23}$$

where

$$q_i = \frac{-\kappa n T_{,i}}{m} . \tag{24}$$

Equation (23) is analogous to the Euler equation for conservation of energy with the driving forces expressed in terms of the electric field and collision terms, with the addition of a heat conduction term. Once again, the definitions of electron internal and total energies per unit mass arise naturally from this transformational procedure.

2.3. Collision terms

The collision terms $[\cdot]_{\text{col}}$ in (1), (2) and (3) describe the rate of change of mass, momentum and energy due to collisions. These terms account for the electron–electron and electron–lattice interactions, the energy transfer between electrons and lattice, and the generation and recombination processes. In the context of one-carrier devices, the case considered in this

paper, the explicit forms given below apply to a ballistic diode problem in which the effects of holes are neglected.

The collision term for the rate of change of mass is due to the generation and recombination processes. These processes are not present in single carrier devices and hence the collision term for the continuity equation is trivial, i.e.,

$$\left[\frac{\partial n}{\partial t}\right]_{\text{col}} = 0 . \tag{25}$$

The collision terms in the momentum conservation, (2), and the energy conservation, (3), represent the rate of change of momentum and energy density, respectively, due to intraband collisions. These are expressed using momentum and energy relaxation times as [3, 6]

$$\left[\frac{\partial p}{\partial t}\right]_{\text{col}} = \frac{-p}{\tau_p} , \qquad \left[\frac{\partial w}{\partial t}\right]_{\text{col}} = \frac{-(w - \frac{3}{2} n k_b T_0)}{\tau_w} , \tag{26}$$

where the momentum relaxation time is expressed as

$$\tau_p = m \frac{\mu_{n0}}{\varepsilon} \frac{T_0}{T} \tag{27}$$

and the energy relaxation time is expressed as

$$\tau_w = \frac{3}{2} \frac{\mu_{n0}}{\varepsilon v_s^2} \frac{k_b T T_0}{T + T_0} + \frac{\tau_p}{2} \tag{28}$$

and v_s is the saturation velocity.

2.4. *Summary of HD equations for a semiconductor device*

In summary, the modified set of HD equations for single carrier devices can be stated as follows:

$$\frac{\partial n}{\partial t} + (n u_i)_{,i} = 0 , \tag{29}$$

$$\frac{\partial}{\partial t}(n u_i) + (n u_i u_j + P \delta_{ij})_{,j} = n \left[-\frac{\varepsilon}{m} E_i - \frac{u_i}{\tau_p} \right] , \tag{30}$$

$$\frac{\partial}{\partial t}(n e_{\text{tot}}) + (n e_{\text{tot}} u_i + P u_i)_{,i} = -\frac{\varepsilon n u_i E_i}{m} - q_{i,i} - \frac{1}{m} \frac{(n m e_{\text{tot}} - \frac{3}{2} n k_b T_0)}{\tau_w} . \tag{31}$$

The HD equations are supplemented by constitutive relations, expressed in terms of thermodynamic quantities, as given below:

(i) The internal energy per unit mass, e_{int}, is defined as

$$e_{\text{int}} = c_v T , \qquad c_v = \frac{3}{2m} k_b , \tag{32}$$

where c_v is the specific heat at constant volume.

(ii) The electron pressure per unit mass, P, can be expressed in terms of γ, the ratio of specific heats, as

$$P = (\gamma - 1) n e_{\text{int}} , \tag{33}$$

where

$$\gamma = \frac{c_p}{c_v} = \frac{5}{3} \quad \text{and} \quad c_p = \frac{5}{2m} k_b . \tag{34}$$

c_p is the specific heat at constant pressure. Equations (32) and (33) constitute the perfect gas law, i.e. they satisfy the relation $Pv = RT$, where $v = 1/n$ is the specific volume and $R = c_p - c_v$ is the specific gas constant.

2.5. *Nondimensionalization of HD equations*

In semiconductor devices, some of the physical quantities of interest are characterized by a very large range in magnitude. Thus, use of dimensional variables may result in ill-conditioning of the matrix problem to be solved. In addition, interpretation of the results may be difficult. This large differential of magnitudes among physical quantities can be addressed by nondimensionalizing the governing equations. Nondimensionalization can be performed on the set of equations (1)–(3) or on (29)–(31) since these two sets of equations are equivalent as shown in the previous sections. Here we discuss the nondimensionalization procedure based on the set (1)–(3).

The conservation laws as defined in (1), (2) and (3) can be made dimensionless if the dependent and independent variables are divided by certain constant reference properties. Some examples of reference properties are the velocity u_0 or the device length L. We select to nondimensionalize the variables as follows:

$$x_i^* = \frac{x_i}{L} , \qquad n^* = \frac{n}{n_0} , \qquad P^* = \frac{P}{n_0 u_0^2} , \qquad u_i^* = \frac{u_i}{u_0} ,$$

$$t^* = \frac{t u_0}{L} , \qquad \nabla^* = L\nabla , \qquad e_{\text{tot}}^* = \frac{e_{\text{tot}}}{u_0^2} , \tag{35}$$

where the dimensionless parameters are denoted by superscript asterisk. All other dimensional parameters are divided by a constant value of its own reference parameter. Using the above scalings, the continuity equation now takes the form

$$\frac{\partial}{\partial t^*} n^* + \nabla^* \cdot (n^* u^*) = 0 . \tag{36}$$

It is noted that the continuity equation has undergone a change of variables under these new transformations. We use a zero collision term for conservation of mass as discussed in Section 2.3. For the conservation of momentum, the nondimensionalized equation takes the form

$$\frac{\partial}{\partial t^*} p^* + u^*(\nabla^* \cdot p^*) + (p^* \cdot \nabla^*) u^*$$

$$= -(\text{Ndp})_1 \varepsilon^* n^* E^* - (\text{Ndp})_2 \nabla^*(n^* k_b^* T^*) + (\text{Ndp})_3 \left[\frac{\partial p}{\partial t} \right]_{\text{col}}^* , \tag{37}$$

where $(\mathrm{Ndp})_1$, $(\mathrm{Ndp})_2$ and $(\mathrm{Ndp})_3$ are three nondimensional parameters defined as

$$(\mathrm{Ndp})_1 = \frac{\varepsilon_0 E_0 L}{m_0 u_0^2}, \qquad (\mathrm{Ndp})_2 = \frac{k_{b0} T_0'}{m_0 u_0^2}, \qquad (\mathrm{Ndp})_3 = \frac{\varepsilon_0 L}{m_0 \mu_{n0}' u_0}. \tag{38}$$

In (38), ε_0 is the reference charge, m_0 is the reference mass, k_{b0} is the reference Boltzmann constant, T_0' is the reference temperature and μ_{n0}' is the reference mobility.

For the energy equation, substituting the nondimensional parameters, we obtain

$$\frac{\partial}{\partial t^*} w^* + \nabla^* \cdot (u^* w^*) = -(\mathrm{Ndp})_1 \varepsilon^* n^* (u^* \cdot E^*)$$
$$-(\mathrm{Ndp})_2 \nabla^* \cdot (u^* n^* k_b^* T^*) - (\mathrm{Ndp})_4 \nabla^* \cdot q^* + (\mathrm{Ndp})_3 \left[\frac{\partial w}{\partial t}\right]_{\mathrm{col}}^*, \tag{39}$$

where

$$(\mathrm{Ndp})_4 = \frac{\kappa_0 T_0'}{m_0 L u_0^3} \tag{40}$$

and κ_0 is the reference conductivity per unit volume. The four nondimensional parameters can be made unity by appropriate selection of reference quantities. In our work, the nondimensional coefficients are made unity by the following choice of reference values:

$$E_0 = \frac{V_t}{L}, \qquad \varepsilon_0 = \frac{\theta_0 V_t}{n_0 L^2}, \qquad k_{b0} = \frac{V_t \varepsilon_0}{T_0'},$$
$$\mu_{n0}' = \frac{u_0 L}{V_t}, \qquad m_0 = \frac{k_{b0} T_0'}{u_0^2}, \qquad \kappa_0 = \frac{\mu_{n0}' k_{b0}^2 T_0'}{\varepsilon_0}. \tag{41}$$

In the above equation, V_t is the reference voltage, θ_0 is the reference permittivity, and all other variables are as defined previously. It can be checked that all nondimensional coefficients are now unity.

In a similar manner, the Poisson equation can be transformed into a nondimensional form as

$$\nabla^* \cdot (\theta^* E^*) = \varepsilon^* (n^* - p^* - N_D^{+*} + N_A^{-*}). \tag{42}$$

Equations (36), (37), (39) and (42) are the nondimensionalized set of device equations that are used in the finite element formulation. For the rest of this paper, we assume that the equations are dimensionless and the asterisk superscript is discarded from our notation for simplicity.

3. Conservation form and symmetrization

In this section we first give the conservation form of the HD equations, which is also known as the divergence law form. The conservation form leads to a quasi-linear system of equations

which involve unsymmetric matrix operators. For this reason we symmetrize the system of equations using entropy functions. Generalized entropy functions for compressible Euler and Navier–Stokes equations have been investigated by Harten [14]. These were enhanced in [10, 15, 16] to account for the heat conduction term. By following the ideas in these previous works, we symmetrize the HD equations. Variational formulations based on the symmetrized systems satisfy the second law of thermodynamics thereby establishing the stability of the solution. As shall be discussed in the next section, symmetrized systems provide the framework for the development of the Galerkin/least-squares method. Additional advantages include improving computational efficiency by employing a linear solver instead of a nonlinear solver, and global conservation under approximate element quadratures.

The HD equations can be written in conservation form as

$$U_{,t} + F_{i,i} = F^h_{i,i} + F \,, \tag{43}$$

where in three dimensions,

$$U = \begin{Bmatrix} U_1 \\ U_2 \\ U_3 \\ U_4 \\ U_5 \end{Bmatrix} = n \begin{Bmatrix} 1 \\ u_1 \\ u_2 \\ u_3 \\ e_{\text{tot}} \end{Bmatrix}, \tag{44}$$

$$F_i = nu_i \begin{Bmatrix} 1 \\ u_1 \\ u_2 \\ u_3 \\ e_{\text{tot}} \end{Bmatrix} + P \begin{Bmatrix} 0 \\ \delta_{1i} \\ \delta_{2i} \\ \delta_{3i} \\ u_i \end{Bmatrix}, \tag{45}$$

$$F^h_i = \begin{Bmatrix} 0 \\ 0 \\ 0 \\ 0 \\ -q_i \end{Bmatrix} \tag{46}$$

and

$$F = \begin{Bmatrix} 0 \\ n\left[-\dfrac{\varepsilon}{m} E_1 - \dfrac{u_1 \varepsilon T}{m\mu_{n0} T_0}\right] \\ n\left[-\dfrac{\varepsilon}{m} E_2 - \dfrac{u_2 \varepsilon T}{m\mu_{n0} T_0}\right] \\ n\left[-\dfrac{\varepsilon}{m} E_3 - \dfrac{u_3 \varepsilon T}{m\mu_{n0} T_0}\right] \\ -\dfrac{\varepsilon n u_i E_i}{m} - \dfrac{1}{m} \dfrac{(nme_{\text{tot}} - \frac{3}{2} nk_b T_0)}{\left[\frac{3}{2} \dfrac{\mu_{n0}}{\varepsilon v_s^2} \dfrac{k_b T T_0}{T + T_0} + \dfrac{\tau_p}{2}\right]} \end{Bmatrix}. \tag{47}$$

It is useful to rewrite the conservation form in the quasi-linear form

$$U_{,t} + A_i U_{,i} = (K_{ij} U_{,j})_{,i} + F \,, \tag{48}$$

where $A_i = F_{i,U}$ and $K_{ij} U_{,j} = F_i^h$. The matrices A_i do not possess the properties of symmetry or positiveness and, in general, are functions of U.

We seek a change of variables $U = U(V)$ to symmetrize the system given in (48) such that each of the coefficient matrices is symmetric. This can be achieved by considering a generalized scalar valued entropy function of the form $\mathcal{H} = \mathcal{H}(U) = -ns$, where s is the thermodynamic entropy per unit mass. We introduce a change of variables $U \rightarrow V$ defined by

$$V^t = \frac{\partial \mathcal{H}}{\partial U} \,, \tag{49}$$

V is referred to as the vector of (physical) entropy variables. In particular, the system is symmetrized by taking

$$s = c_v \ln\left(\frac{P}{P_0}\left(\frac{n}{n_0}\right)^{-\gamma}\right) + s_0 \,, \tag{50}$$

where s_0 is the reference entropy, n_0 and P_0 are reference concentration and pressure, respectively. The new variables V^t are computed by using the chain rule

$$V^t = \mathcal{H}_{,U} = \mathcal{H}_{,Y}(U_{,Y})^{-1} \,, \tag{51}$$

where

$$Y = \begin{Bmatrix} v \\ u \\ e_{\text{int}} \end{Bmatrix} \tag{52}$$

and v is the specific volume. Using the definition of Y, we obtain

$$\mathcal{H}_{,Y} = \begin{bmatrix} \dfrac{s-R}{v^2} & 0 & 0 & 0 & -\dfrac{1}{vT} \end{bmatrix} \tag{53}$$

and

$$U_{,Y} = \begin{bmatrix} -\dfrac{1}{v^2} & 0 & 0 & 0 & 0 \\ -\dfrac{u_1}{v^2} & \dfrac{1}{v} & 0 & 0 & 0 \\ -\dfrac{u_2}{v^2} & 0 & \dfrac{1}{v} & 0 & 0 \\ -\dfrac{u_3}{v^2} & 0 & 0 & \dfrac{1}{v} & 0 \\ -\dfrac{e_{\text{tot}}}{v^2} & \dfrac{u_1}{v} & \dfrac{u_2}{v} & \dfrac{u_3}{v} & \dfrac{1}{v} \end{bmatrix}. \tag{54}$$

The new entropy variables are thus obtained from (51) as

$$V = \frac{1}{T}\begin{Bmatrix} \mu - \frac{1}{2}|u|^2 \\ u_1 \\ u_2 \\ u_3 \\ -1 \end{Bmatrix}, \tag{55}$$

where $\mu = e_{\text{int}} + Pv - Ts$ is the specific chemical potential.

Using the change of variables, the system of equations given in (48) can be rewritten as

$$\tilde{A}_0 V_{,t} + \tilde{A}_i V_{,i} = (\tilde{K}_{ij} V_{,j})_{,i} + F\,, \tag{56}$$

where

$$\tilde{A}_0 = U_{,V}\,, \qquad \tilde{A}_i = A_i \tilde{A}_0\,, \qquad \tilde{K}_{ij} = K_{ij}\tilde{A}_0\,. \tag{57}$$

In the above definitions, $\tilde{A}_0$ is symmetric and positive definite and $\tilde{A}_i$ is symmetric. The explicit definitions of all the coefficient matrices are summarized in Appendix A. These coefficient matrices are first given in [16] for the compressible Euler and Navier–Stokes equations.

In addition to the matrices defined above, it is useful to express the source vector as a product of a coefficient matrix $\tilde{C}$ and the vector V:

$$F = -\tilde{C}V\,. \tag{58}$$

The definition of $\tilde{C}$ is not unique. In Appendix A, we have included one possible definition of $\tilde{C}$ which is symmetric and positive definite.

4. Finite element formulation

This section presents a finite element formulation for the HD equations and the Poisson equation. For the HD equations, we enhance the space-time finite element formulations developed for compressible Navier-Stokes equations to account for the highly nonlinear source terms. The standard Galerkin finite element method is employed for the Poisson equation.

4.1. Finite element method for HD equations

The standard Galerkin finite element method exhibits spurious oscillations and poor stability properties for advective–diffusive systems in which the exact solution may be nonsmooth or discontinuous [8]. This deficiency led to the development of the Streamline-Upwind/Petrov–Galerkin (SUPG) method, which exhibits good stability properties and higher order accuracy [9, 17, 18]. The essential idea in the SUPG method is the addition of stabilizing terms, which introduces artificial diffusion in the Galerkin method to provide control over the advective derivative term. Since SUPG is a higher order linear method, monotone approximations of sharp layers is not possible. Thus some undershoot and/or overshoot may appear in the solution. Nonlinear shock capturing operators have been developed to overcome these undershoot and/or overshoot problems [10, 19, 20].

Galerkin/least-squares finite element methods are simple extensions to SUPG methods [21]. The methods coincide with SUPG methods in the absence of diffusion and source terms, and provide a more general framework than SUPG methods in the presence of diffusion and source terms. Terms of a least-squares type are added to the Galerkin method to obtain stability. The least-squares terms vanish at the exact solution thus establishing consistency.

The temporal behavior of the problem is accounted for by using a discontinuous in time Galerkin approximation [25]. In the space-time Galerkin/least-squares method, the solution is obtained by marching sequentially through time; the solution of the system of equations at each time step is computed based on the solution obtained at the previous time step. In the following we develop the variational equation and then the finite element discretization for steady state problems.

4.1.1. Variational formulation

Let $0 = t_0 < t_1 < \cdots < t_N = T$ be a sequence of time levels and $Q_n = \Omega \times I_n$ be a sequence of time-slabs in which Ω is the spatial domain and $I_n = (t_n, t_{n+1})$ is a time interval. Let $(n_{el})_n$ denote the number of space-time elements in Q_n, and $Q_n^e = \Omega_n^e \times I_n$ denote the space time element domain in the nth time slab with Ω_n^e the discretization of the spatial domain in the nth time slab. The space of trial functions is

$$\mathcal{S}_n^h = \{V^h \mid V^h \in H^1(Q_n), D(V^h) = g(t) \text{ on } B_n\}, \tag{59}$$

where $B_n = \Gamma \times I_n$ denotes the boundary of the nth space time slab, D is the nonlinear boundary operator, and g is the prescribed boundary condition. The space of weighting functions is

$$\mathcal{V}_n^h = \{W^h \mid W^h \in H^1(Q_n), D'(W^h) = 0 \text{ on } B_n\}, \tag{60}$$

where D' is the nonlinear boundary condition operator.

Before stating the variational equation, it is useful to introduce the following notation:

$$(W^h, V^h)_{Q_n} = \int_{Q_n} (W^h \cdot V^h)\, dQ, \tag{61}$$

$$(W^h, V^h)_{\Omega} = \int_{\Omega} (W^h \cdot V^h)\, d\Omega, \tag{62}$$

$$a(W^h, V^h)_{Q_n} = \int_{Q_n} (W_{,i}^h \cdot \tilde{K}_{ij} V_{,j}^h)\, dQ, \tag{63}$$

$$(W^h, V^h)_{B_n} = \int_{B_n} (W^h \cdot V^h) n_i\, dB, \tag{64}$$

$$(W^h, V^h)_{Q_n^\Sigma} = \sum_{e=1}^{(n_{el})_n} \int_{Q_n^e} (W^h \cdot V^h)\, dQ. \tag{65}$$

The space-time Galerkin/least-squares formulation for the symmetrized electron system equation (56) can be stated as follows. Within each Q_n, $n = 0, \ldots, n-1$, find $V^h \in \mathcal{S}_n^h$ such

that for all $W^h \in \mathcal{P}_n^h$ the following variational equation is satisfied:

$$B_{GLS}(W^h, V^h)_n = L_{GLS}(W^h)_n , \tag{66}$$

where

$$B_{GLS}(W^h, V^h)_n = B(W^h, V^h)_n + (\mathcal{L}W^h, \tau\mathcal{L}V^h)_{Q_n^\Sigma} + B_{DC}(W^h, V^h) , \tag{67}$$

$$B(W^h, V^h)_n = (-W_{,t}^h, U(V^h))_{Q_n} + (W_{,i}^h, F_i(V^h))_{Q_n} + a(W^h, V^h)_{Q_n} + (W^h, F(V^h))_{Q_n} + (W^h(t_{n+1}^-), U(V^h(t_{n+1}^-)))_\Omega + (W^h, F_i(V^h) - F_i^h(V^h))_{B_n} , \tag{68}$$

$$B_{DC}(W^h, V^h) + (v^h \hat{\nabla}_\xi W^h, [[\hat{A}_0]] \hat{\nabla}_\xi V^h)_{Q_n^\Sigma} , \tag{69}$$

$$L_{GLS}(W^h)_n = L(W^h)_n = (W^h(t_n^+), U(V^h(t_n^-)))_\Omega . \tag{70}$$

With regard to (67)–(70), the following remarks are applicable:

(i) The first term on the right-hand-side of (67) constitutes the time-discontinuous Galerkin formulation, which is given in (68).

(ii) The second integral product in (67) is the least-squares operator which is nonlinear in both W^h and V^h. The symmetric positive semidefinite, $n_{dof} \times n_{dof}$ matrix τ contains Galerkin/least-squares parameters whose selection is discussed in [22]. τ can be interpreted as a matrix of intrinsic time scales. The number of degrees of freedom of the problem are n_{dof}, and $\mathcal{L}$ is the governing differential operator of the problem defined from (56) as

$$\mathcal{L} = \tilde{A}_0 \frac{\partial}{\partial t} + \tilde{A}_i \frac{\partial}{\partial x_i} - \frac{\partial}{\partial x_i}\left(\tilde{K}_{ij} \frac{\partial}{\partial x_j}\right) + \tilde{C} . \tag{71}$$

(iii) The third term in (67) is a discontinuity-capturing operator and is also nonlinear in both W^h and V^h. The integral product definition of this term is given in (69). $\hat{\nabla}_\xi$ is defined as the generalized local coordinates gradient operator. v^h is a scalar discontinuity-capturing factor having the dimension of reciprocal of time, and

$$[[\tilde{A}_0]] = \begin{bmatrix} \tilde{A}_0 & & & \\ & \tilde{A}_0 & & \\ & & \ddots & \\ & & & \tilde{A}_0 \end{bmatrix} . \tag{72}$$

The selection of v^h has been discussed in [10].

(iv) Equation (70) is the contribution of the jump condition term. Jump condition is added to the variational form to enforce weak initial conditions for each space–time slab, and introduce numerical dissipation. The jump condition is given by

$$\int_\Omega W^h(t_n^+) \cdot \lceil\lfloor U(V^h(t_n))\rfloor\rceil \, d\Omega , \tag{73}$$

where

$$\lceil\lfloor U(t_n)\rfloor\rceil = U(t_n^+) - U(t_n^-) \tag{74}$$

denotes the jump in time of U.

4.1.2. Finite element discretization

A computationally efficient scheme for steady state problems can be developed by considering the finite element spaces to be constant in time within each space–time slab and discontinuous across the space–time slab interfaces. Within the nth space–time slab, the finite element trial solution and the weighting function are taken to be

$$V^h = \sum_{A=1}^{(n_{np})_n} N_A^{(n)}(x) v_{A;(n+1)}, \qquad W^h = \sum_{A=1}^{(n_{np})_n} N_A^{(n)}(x) w_{A;(n+1)}, \quad \text{for } x \in \Omega, \tag{75}$$

where $v_{A;(n+1)}$ and $w_{A;(n+1)}$ are, respectively, the $n_{dof} \times 1$ vectors of nodal unknowns and weighting functions at node A for the nth space–time slab. $(n_{np})_n$ is the number of nodal points for the nth space–time slab, and $N_A^{(n)}(x)$ is the finite element spatial shape-function of node A for the nth space–time slab (the subscripts and superscripts are dropped from now on to simplify the notation). Defining

$$v = \{v_A^t\}^t, \qquad w = \{w_A^t\}^t, \qquad v_n = \{v_{A;n}^t\}^t, \quad A = 1, \ldots, n_{np}, \tag{76}$$

and substituting the finite element approximations (75), into the space–time Galerkin/least-squares variational equation (66), we obtain

$$w \cdot G(v; v_{(n)}) = 0, \tag{77}$$

where $G(v; v_{(n)})$ is a system of nonlinear algebraic equations with an unknown vector v. Since (77) must hold for all unconstrained coefficients w, it follows that

$$G(v; v_{(n)}) = 0. \tag{78}$$

Equation (78) is the nonlinear finite element matrix equation in which there are $n_{np} \times n_{dof}$ equations and $n_{np} \times n_{dof}$ unknowns.

The nonlinear system can be linearized with respect to the unknown vector v, and a time stepping solution algorithm can be employed in the format of the predictor multi-corrector algorithm. At each time slab n, if we denote $v^{(i)}$ to be the ith iterative approximation of $v_{(n+1)}$, with $v^{(0)} = v_{(n)}$, linearization of (78) gives

$$R^{(i)} + M^{(i)} \Delta v^{(i)} = 0, \tag{79}$$

where

$$\Delta v^{(i)} = v^{(i)} - v^{(i-1)}. \tag{80}$$

$R^{(i)}$ and $M^{(i)}$ denote the residual vector and the consistent tangent matrix at the ith iteration, respectively. The predictor multi-corrector algorithm can now be summarized as follows:

For each time step, n, do
begin

Predictor: $\boldsymbol{v}^{(0)} = \boldsymbol{v}_{(n)}$;
For each corrector $i = 0, 1, \ldots, n_{\text{cor}} - 1$ *do*
begin /* *corrector loop* */
$\quad$ *solve* $\boldsymbol{M}^{(i)} \Delta \boldsymbol{v}^{(i)} = -\boldsymbol{R}^{(i)}$;
$\quad \boldsymbol{v}^{(i+1)} = \boldsymbol{v}^{(i)} + \Delta \boldsymbol{v}^{(i)}$;
end.
$\boldsymbol{v}_{(n+1)} = \boldsymbol{v}^{(n_{\text{cor}})}$;
end.

In the above procedure, n_{cor} denotes the number of correctors.

4.2. *Finite element model for the Poisson equation*

Finite element formulation of the Poisson equation given in (7) is rather straightforward and is briefly summarized in this section. The space of the trial functions is

$$\mathcal{S}_1^h = \{\psi^h \mid \psi^h \in H^1(\Omega),\ \psi^h = g_p \text{ on } \Gamma_g\} \tag{81}$$

and the space of weighting functions is

$$\vartheta_1^h = \{\bar{\psi}^h \mid \bar{\psi}^h \in H^1(\Omega),\ \bar{\psi}^h = 0 \text{ on } \Gamma_g\}\,, \tag{82}$$

where g_p are the prescribed essential boundary conditions applied at the boundary Γ_g.

The weak form of the problem can be stated as follows: Find $\psi^h \in \mathcal{S}_1^h$ such that for all $\bar{\psi}^h \in \vartheta_1^h$, the following equation is satisfied:

$$\int_\Omega \left(\frac{\partial \bar{\psi}^h}{\partial x_i} \frac{\partial \psi^h}{\partial x_i} + \bar{\psi}^h e(n - p - N_D^+ + N_A^-) \right) d\Omega - \int_{\Gamma_h} \bar{\psi}^h h_i \, d\Gamma = 0\,, \tag{83}$$

where $(\partial \psi^h / \partial x_i) k_i = h_i$ are the natural boundary conditions prescribed on the portion of the boundary Γ_h, and k_i denotes the unit outward normal to the boundary Γ_h.

Using standard finite element discretization [23], a matrix form is obtained which is solved for the potential ψ^h at all nodes. The electric fields are computed at the center of each element and then projected onto the mesh nodes using smoothing procedures of a least-squares type [24].

5. Solution schemes

This section discusses an algorithmic approach for solving coupled HD and Poisson equations. One approach is to solve the coupled HD and Poisson problems simultaneously. However, for the one-carrier devices that we consider in this paper, the coupling between the electron HD equations and the Poisson equation is through the source terms. The collision terms presented in Section 2.3 do not couple with the Poisson equation. A staggered scheme appears attractive for this weakly coupled system of Poisson and HD equations. Computation-

ally, the staggered scheme that treats the Poisson equation and the HD equations separately is more efficient than solving both equations as a single system.

In the staggered scheme, we first solve the Poisson equation for the potential and electric fields. We use the computed electric fields and solve the HD equations for concentrations, velocities and temperature. The computed concentrations are then taken as input for the Poisson equation to calculate the electric fields. This iterative procedure is stopped when all the equations are satisfied within a given tolerance parameter for convergence. Although we have not pursued mathematical proofs for stability of the staggered scheme, our experience on the test examples presented in the next section indicate that this solution scheme is quite stable.

The solution is said to reach a steady state when the residual is constant and does not decrease any further. The constant in time approximation for finite element spaces provides a very attractive time marching scheme for steady state problems. This scheme, however, provides low order of accuracy in time and may not be considered sufficiently accurate for transient problems. For transient problems, high order of accuracy in time can be provided by employing linear in time finite element spaces; this subject is beyond the scope of this paper.

6. Numerical results

The numerical algorithms presented in the previous sections are tested for one- and two-dimensional single-carrier devices. This section describes the results obtained to illustrate the applicability of the finite element formulation for semiconductor device problems. First, we will treat a traditional example, an n^+-n-n^+ silicon diode, to verify the results of our code against those reported in literature. Next, we will discuss a simple extension of this problem to a 2-D problem. The intention is to show the generality of our approach; no modifications in our formulation need to be made to deal with 2-D and/or 3-D problems. In a future paper, we will report on results for more complex and more interesting devices. Here, we focus on the numerical capabilities of the proposed finite element formulation.

6.1. *Example 1: 1-D problem*

Computational experiments are performed on a 0.6-μm n^+-n-n^+ silicon diode at 300 K with $n^+ = 5.0 \times 10^{17}\ \mathrm{cm}^{-3}$ and $n = 2.0 \times 10^{15}\ \mathrm{cm}^{-3}$. The doping in the n^+-n transition region varies as a Gaussian function with a $\sigma = 0.01\ \mu\mathrm{m}$, the length of the n-region is approximately 0.4 μm. The boundary conditions applied are given as follows:

$$\text{at } x = 0\ \mu\mathrm{m}, \quad n = 5.0 \times 10^{17}\ \mathrm{cm}^{-3}, \quad T = T_0 = 300\ \mathrm{K}, \quad \psi = \psi_b(n_d);$$

$$\text{at } x = 0.6\ \mu\mathrm{m}, \quad n = 5.0 \times 10^{17}\ \mathrm{cm}^{-3}, \quad T = T_0 = 300\ \mathrm{K}, \quad \psi = \psi_b(n_d) + \psi_{\mathrm{appl}}.$$

ψ_b is the built-in potential defined as

$$\psi_b = \frac{k_b T}{\varepsilon} \ln\left(\frac{n_d}{n_i}\right),$$

where n_d is the doping and n_i is the intrinsic concentration. ψ_{appl} denotes the applied bias which is taken as 1.5 V or 2.0 V (we show numerical results for both cases). The initial conditions for the time-marching scheme that we employ to reach steady state are as follows:

$$\text{at } t = 0\,, \quad n(x,0) = n_d(x)\,, \quad u(x,0) = 0.0\,, \quad T(x,0) = T_0\,.$$

In these results, no continuation method is used, i.e. the bias is applied in a single load step. We used 101 mesh points for this problem and with this mesh size, the least-squares terms are sufficient to smooth the solution near discontinuities, i.e. we do not need to use shock capturing operators.

The steady state results for this problem are shown in Figs. 1–5. Our results agree very well with the results previously reported in the literature [2, 5–7]. It should be noted here that, although the physical 'truth' of these solutions is still being debated, the numerical results obtained in this study prove the accuracy of our formulation and therefore support the notion that this formulation can very well be used to investigate exactly what would be the right physical model formulation.

6.2. *Example 2: 2-D problem*

Our two-dimensional example is a simple extension of the one-dimensional problem discussed above. The geometry of the device is shown in Fig. 6. The dark lines indicate the contact positions. Contacts 4–5 and 4–6 are terminated at a distance of 0.07 μm from the top left corner. The doping profile is given by

$$n_d(x, y) = 5.0 \times 10^{17}\ \text{cm}^{-3}\,, \quad \text{for } 0.0 \leq x \leq 0.6 \text{ and } 0.0 \leq y \leq 0.1\,,$$

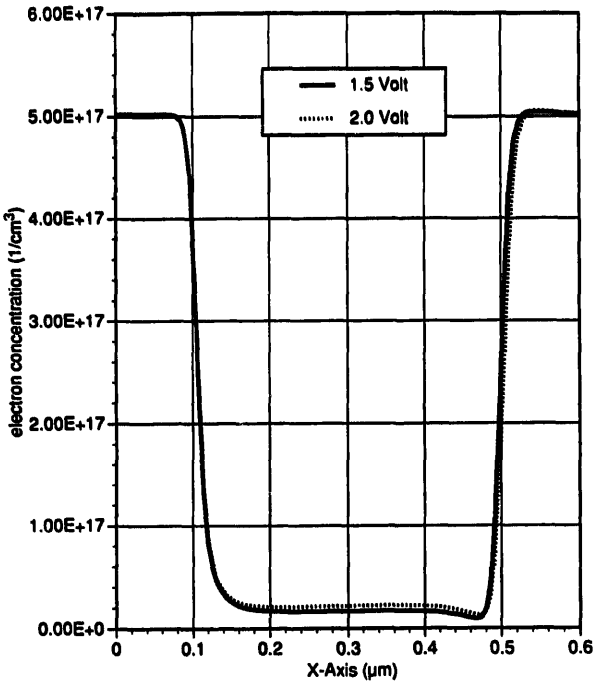

Fig. 1. Electron concentration (cm^{-3}) in steady state.

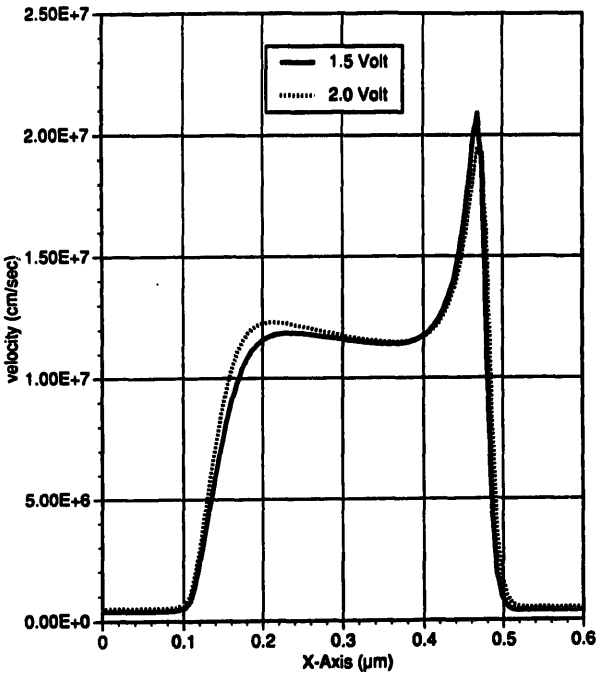

Fig. 2. Electron velocity (cm/s) in steady state.

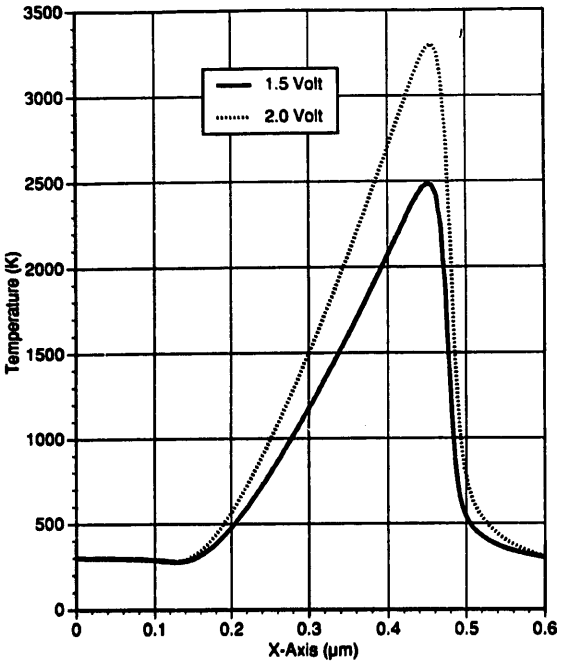

Fig. 3. Temperature (K) in steady state.

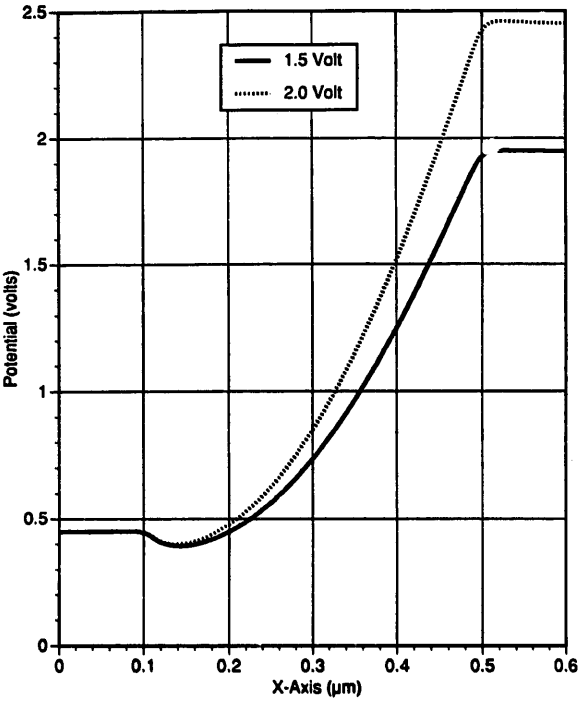

Fig. 4. Electrostatic potential (V) in steady state.

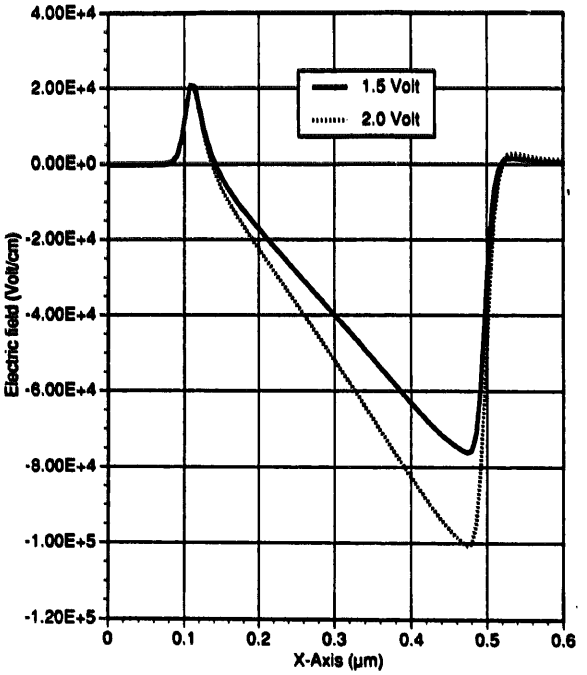

Fig. 5. Electric field (V/cm) in steady state.

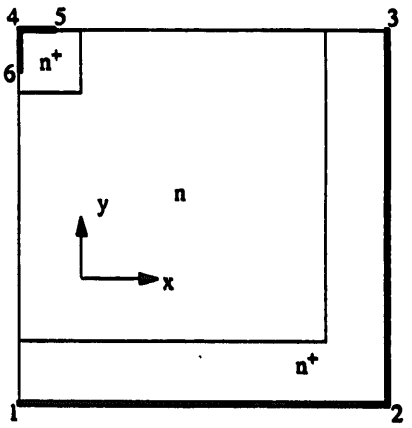

Fig. 6. A 0.6 μm × 0.6 μm n^+-n-n^+ silicon device. Contacts are denoted by dark lines.

$$n_d(x, y) = 5.0 \times 10^{17}\ \text{cm}^{-3}, \quad \text{for } 0.5 \leq x \leq 0.6 \text{ and } 0.2 \leq y \leq 0.6,$$

$$n_d(x, y) = 5.0 \times 10^{17}\ \text{cm}^{-3}, \quad \text{for } 0.0 \leq x \leq 0.1 \text{ and } 0.5 \leq y \leq 0.6,$$

$$n_d(x, y) = 2.0 \times 10^{15}\ \text{cm}^{-3}, \quad \text{elsewhere, with abrupt junctions.}$$

The boundary conditions we used for this problem are summarized as follows:

(i) along contact 1–2: $n(x, 0) = n_d(x, 0)$, $u(x, 0) = 0.0$, $T(x, 0) = T_0 = 300$ K, and $\psi(x, 0) = \psi_b + 1.0$ V.

(ii) along contact 2–3: $n(0.6, y) = n_d(0.6, y)$, $v(0.6, y) = 0.0$, $T(0.6, y) = 300$ K, and $\psi(0.6, y) = \psi_b + 1.0$ V.

(iii) along contact 4–5: $n(x, 0.6) = n_d(x, 0.6)$, $u(x, 0.6) = 0.0$, $T(x, 0.6) = 300$ K, and $\psi(x, 0.6) = \psi_b$.

(iv) along contact 4–6: $n(0, y) = n_d(0, y)$, $v(0, y) = 0.0$, $T(0, y) = 300$ K, and $\psi(0, y) = \psi_b + 1.0$ V.

(v) along boundary 5–3: $v = 0.0$, and Neumann boundary conditions for temperature and potential.

(vi) along boundary 6–1: $u = 0.0$ and Neumann boundary conditions for temperature and potential.

The initial conditions are taken as $n(x, y) = n_d(x, y)$, $u(x, y) = v(x, y) = 0.0$, and $T(x, y) = T_0 = 300$ K. We use a relatively coarse grid of 61×61 mesh points. The steady-state results for this problem are shown in Figs. 7–13. In order to simulate a realistic device, contacts are not extended to the full n^+ region near the top left corner as shown in Fig. 6.

In Fig. 8, the horizontal velocity u obtained at the steady state is shown. As expected, the solution along the line $y = 0.6$ μm is very similar to the 1-D case. The global pattern of the solution can easily be understood from the 2-D character of the problem. There are two small

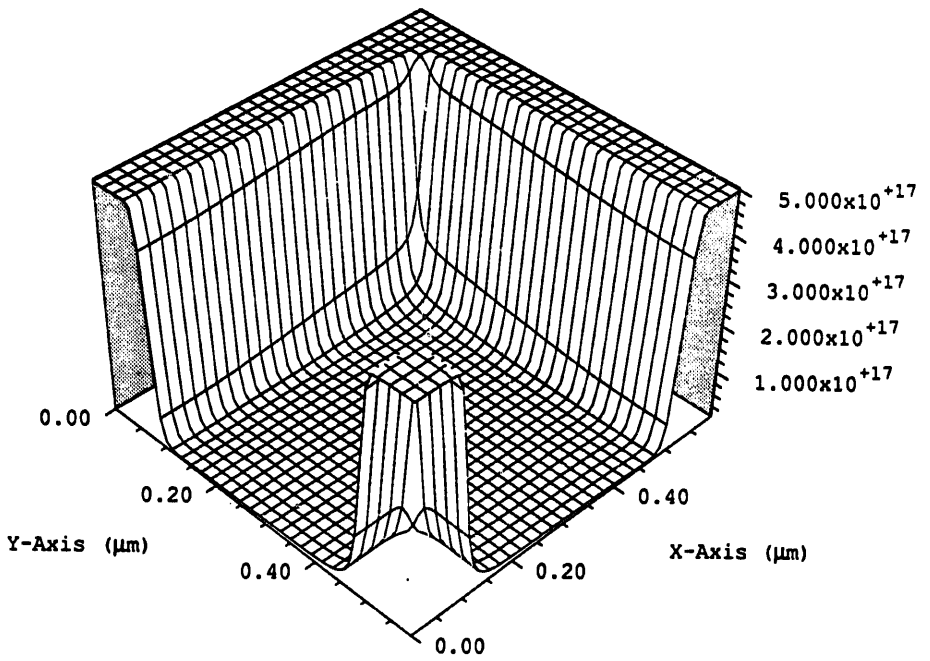

Fig. 7. Electron concentration (cm^{-3}) in steady state.

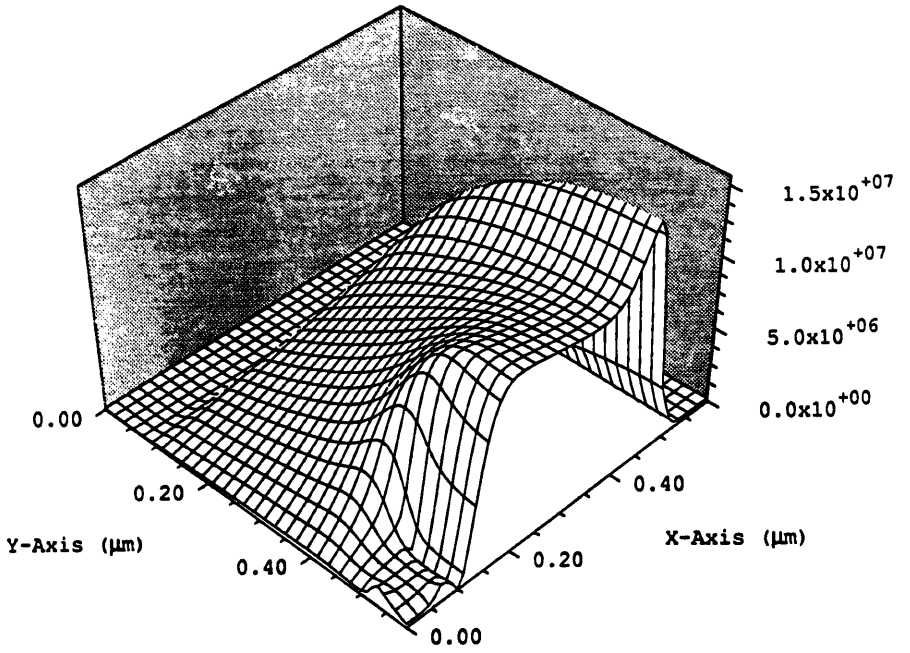

Fig. 8. Horizontal velocity (cm/s) in steady state.

details in the solution that need explanation, namely the small peaks in the velocity very close to the front corner of the device along both axes, between the edge of the contact and the boundary of the n^+ doping region. The peak along the x-axis is field driven. The electrons come out of the contact along the x-axis with in essence only a velocity in the y-direction. Those electrons entering the device very close to the end of the x-axis contact are immediately

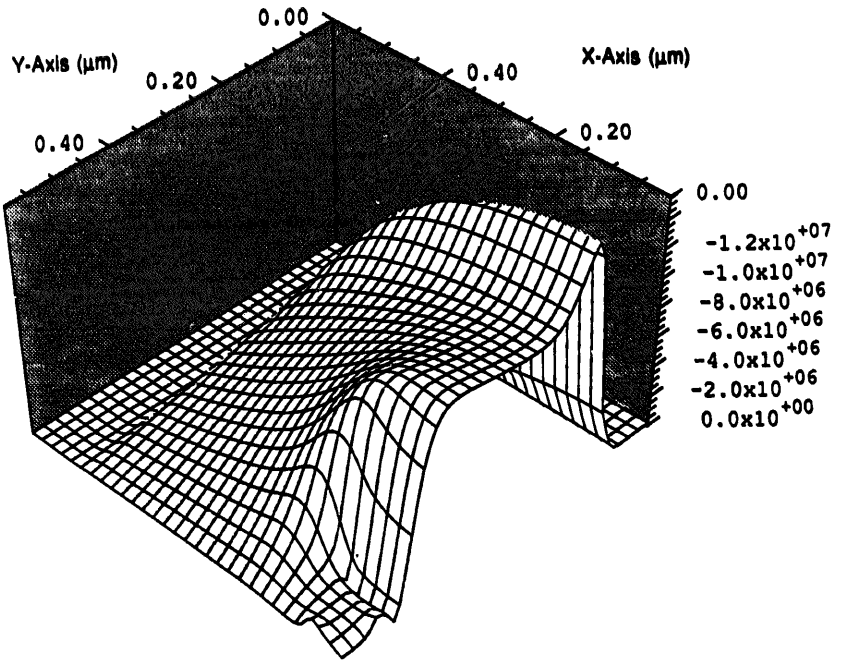

Fig. 9. Vertical velocity (cm/s) in steady state.

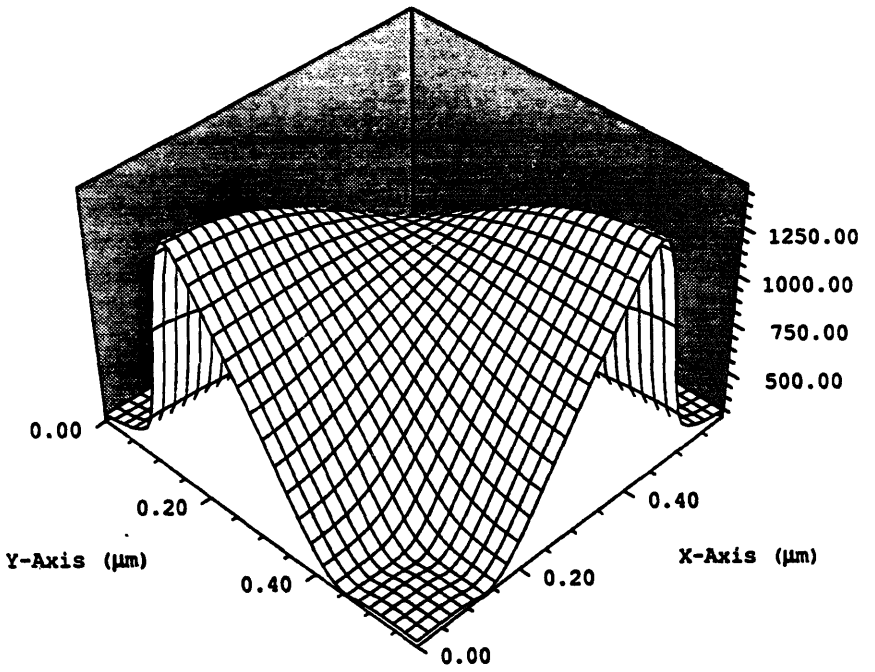

Fig. 10. Temperature (K) in steady state.

accelerated into the x-direction by the built-in electrical field in the diode junction. This explains the little bump in the x-velocity to the right of the x-axis contact. The peak along the y-axis has a different origin. Here, we are dealing with electrons streaming out of the y-axis contact and therefore with a tendency to pick up good x-velocity. The electrons coming out of this contact very close to the corner are, however, hampered in picking up speed because they

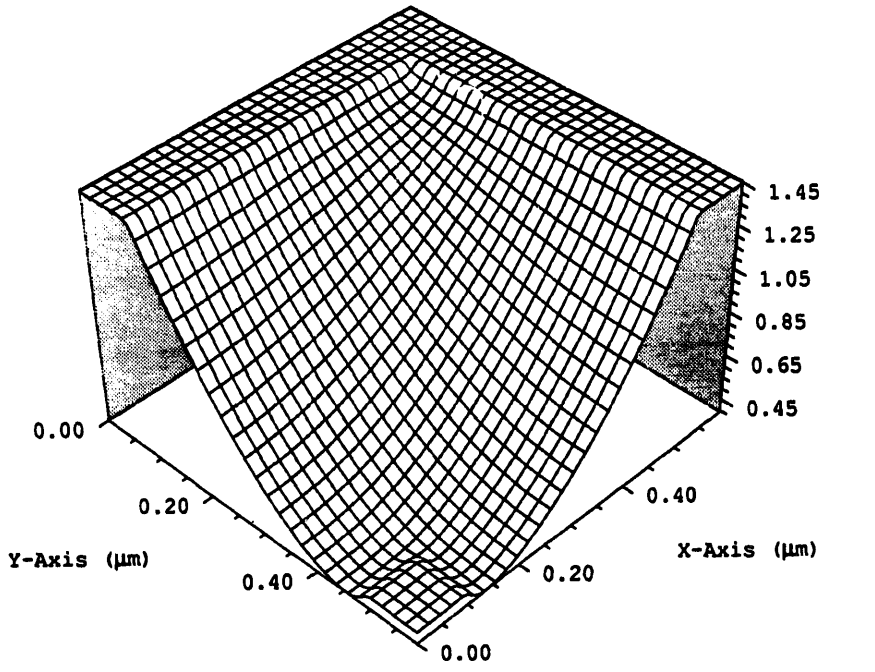

Fig. 11. Electrostatic potential (V) in steady state.

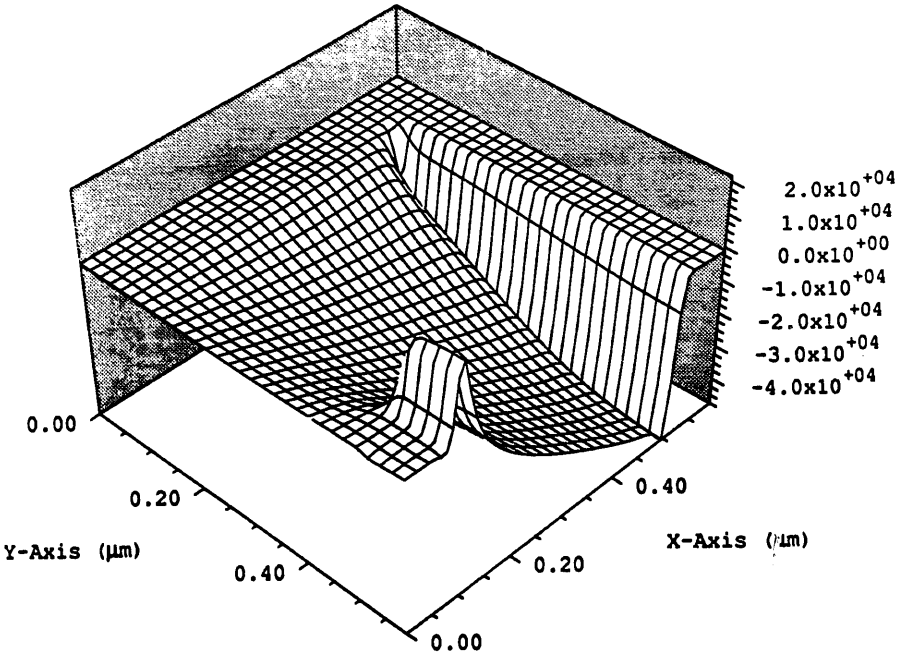

Fig. 12. Horizontal component of electric field (V/cm) in steady state.

'collide' with the electrons coming out of the x-axis contact close to the corner. The further we go along the y-axis away from the corner, the less this 'hampering' effect becomes as evidenced by the corresponding increase in x-velocity. Figure 9 shows the y-velocity. As expected from the symmetry of the problem, the profile is as good as identical to the one for x-velocity. Also the temperature data relate very well to the 1-D solutions and therefore are

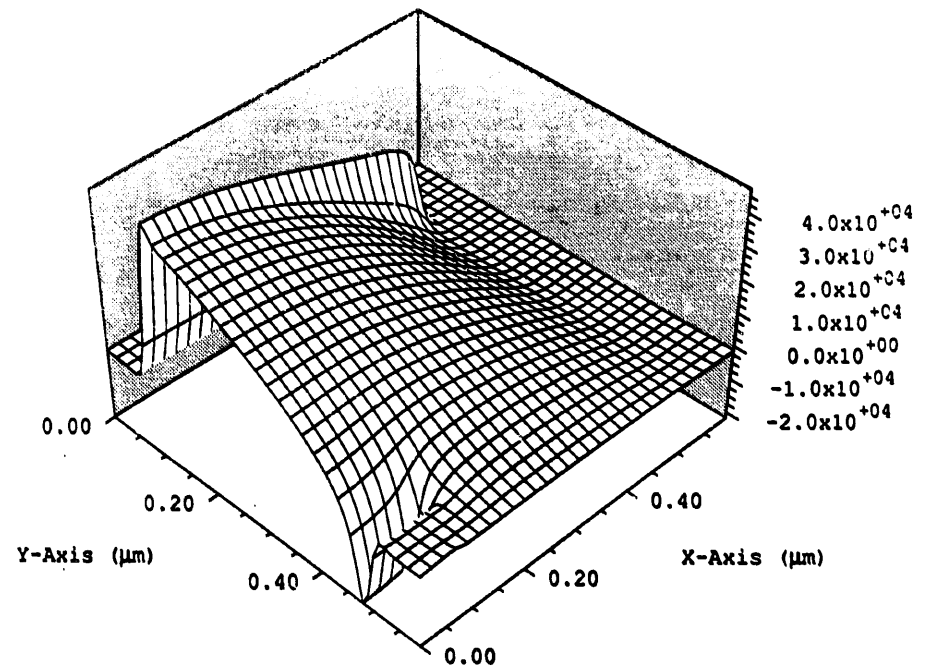

Fig. 13. Vertical component of electric field (V/cm) in steady state.

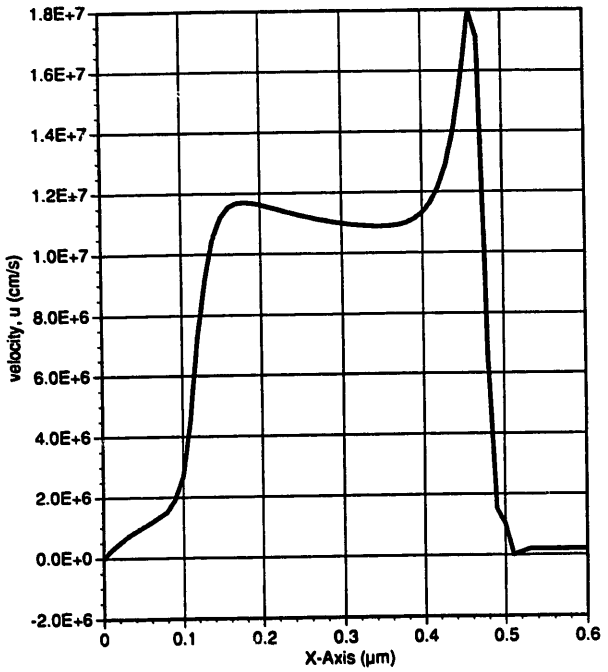

Fig. 14. Horizontal component of velocity along $y = 0.490$ without shock capturing operator.

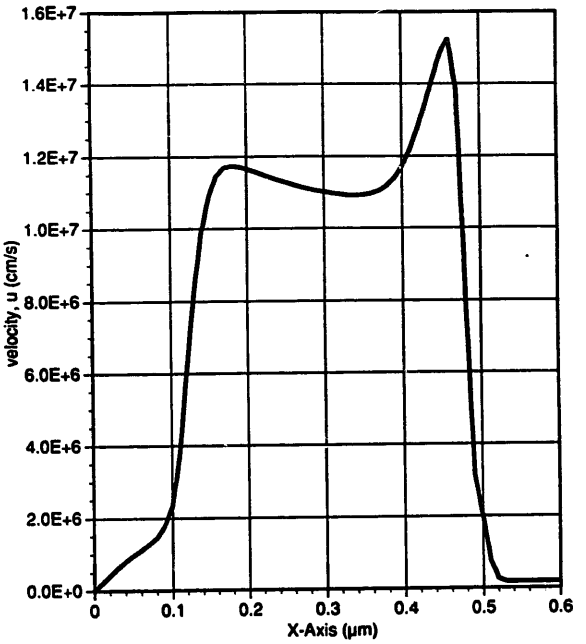

Fig. 15. Vertical component of velocity along $y = 0.490$ with shock capturing operator.

assumed to be accurate. Once again, we did not need to use the continuation method and the entire data bias specified is applied in a single step. However, in this example we need to use the shock capturing operators to eliminate small undershoots and overshoots given the coarseness of the mesh. In Figs. 14 and 15, horizontal component of velocity along $y = 0.490$ with and without shock capturing operators, respectively, are shown.

7. Summary

In this paper a general space–time Galerkin/least-squares finite element formulation for solving the HD equations of semiconductor devices is presented. Nonlinear shock capturing operators developed in the context of fluid flow problems have been enhanced to accommodate the highly nonlinear source terms present in the HD model, and were found to be useful to eliminate undershoots and overshoots near discontinuities. Numerical results reveal velocity overshoot, consistent with previously reported data. It is interesting to note that the heat flux term plays an important role in the simulation of velocity overshoot. When the heat flux term is neglected, unreasonable results with no velocity overshoot are observed. Well posed boundary conditions for 2D and 3D hydrodynamic models for semiconductor device problems are not clearly understood, contrary to the situation for compressible Euler and Navier–Stokes equations. This can be attributed to the need for a velocity boundary condition at a contact, which seems unphysical for device simulation. In our numerical studies, we found our algorithms to be stable even when we did not specify mathematically adequate boundary conditions. Specification of well posed, and physical boundary conditions is an area that requires further investigation.

The method described in this paper for semiconductor device equations is computationally very expensive. Current and future work will involve parallelizing the finite element software on multi-processing architecture, solving two-carrier devices in 2D as well as 3D, and developing an adaptive version of the finite element method.

Appendix A. Coefficient matrices

In this appendix, we present the flux vectors and the coefficient matrices of the hydrodynamic equations, as expressed in terms of the (physical) entropy variables.

For referential convenience, the mapping from U to V is provided here:

$$V = \frac{1}{T}\begin{Bmatrix} \mu - \dfrac{|u|^2}{2} \\ u_1 \\ u_2 \\ u_3 \\ -1 \end{Bmatrix} = \frac{v}{T}\begin{Bmatrix} -U_5 + \dfrac{T}{v}[(\gamma+1)c_v - s] \\ U_2 \\ U_3 \\ U_4 \\ -U_1 \end{Bmatrix}, \tag{A.1}$$

where

$$s = c_p \ln \frac{T}{T_0} - R \ln \frac{P}{P_0} + s_0 , \tag{A.2}$$

$$\frac{T}{v} = \frac{1}{c_v}\left[U_5 - \frac{U_2^2 + U_3^2 + U_4^2}{2U_1}\right]. \tag{A.3}$$

The inverse mapping $V \rightarrow U$ is given as

$$U = \frac{1}{v}\begin{Bmatrix} 1 \\ u_1 \\ u_2 \\ u_3 \\ e_{int} + \dfrac{|u|^2}{2} \end{Bmatrix} = \frac{T}{v}\begin{Bmatrix} -V_5 \\ V_2 \\ V_3 \\ V_4 \\ c_v - \dfrac{(V_2^2 + V_3^2 + V_4^2)}{2V_5} \end{Bmatrix}, \tag{A.4}$$

where

$$\frac{T}{v} = K^{1/R} \frac{1}{(-V_5)^{c_p/R}} \exp\left(\frac{-s + s_0}{R}\right), \qquad K = \frac{\left(\dfrac{P_0}{R}\right)^R}{(T_0)^{c_p}}, \tag{A.5}$$

$$s = \gamma c_v - V_1 + \frac{V_2^2 + V_3^2 + V_4^2}{2V_5}. \tag{A.6}$$

The coefficient matrices are expressed with the help of the following variables:

$$h = c_p T, \qquad e_{int} = c_v T, \qquad \alpha_p = \frac{1}{T}, \qquad \beta_T = \frac{1}{P}, \qquad c_p - c_v = R, \tag{A.7}$$

$$k = \frac{|u|^2}{2}, \qquad d = \frac{v\alpha_p T}{\beta_T}, \qquad \bar{\gamma} = \frac{v\alpha_p}{\beta_T c_v}, \tag{A.8}$$

$$c_1 = u_1^2 + \frac{v}{\beta_T}, \qquad c_2 = u_2^2 + \frac{v}{\beta_T}, \qquad c_3 = u_3^2 + \frac{v}{\beta_T}, \tag{A.9}$$

$$\bar{c}_1 = u_1^2 + c_v T, \qquad \bar{c}_2 = u_2^2 + c_v T, \qquad \bar{c}_3 = u_3^2 + c_v T, \tag{A.10}$$

$$e_1 = h + k, \qquad e_2 = e_1 - d, \qquad e_3 = e_2 + \frac{v}{\beta_T}, \qquad e_4 = e_2 + 2\frac{v}{\beta_T}, \tag{A.11}$$

$$\bar{e}_1 = h - k, \qquad \bar{e}_2 = \bar{e}_1 - d, \qquad \bar{e}_3 = \bar{e}_2 - c_v T, \qquad a^2 = \frac{v c_p}{c_v \beta_T}, \tag{A.12}$$

$$u_{12} = u_1 u_2, \qquad u_{23} = u_2 u_3, \qquad u_{31} = u_3 u_1, \qquad u_{123} = u_1 u_2 u_3, \tag{A.13}$$

$$e_5 = e_1^2 - 2e_1 d + \frac{v(2k + c_p T)}{\beta_T}, \qquad \bar{e}_5 = \bar{e}_1^2 - 2\bar{e}_1 d + 2kc_v T + \frac{v c_p T}{\beta_T}, \tag{A.14}$$

$$\tilde{A}_0 = \frac{\beta_T T}{v^2}\begin{bmatrix} 1 & u_1 & u_2 & u_3 & e_2 \\ & c_1 & u_{12} & u_{31} & u_1 e_3 \\ & & c_2 & u_{23} & u_2 e_3 \\ & \text{symm} & & c_3 & u_3 e_3 \\ & & & & e_5 \end{bmatrix}, \tag{A.15}$$

$$\tilde{A}_0^{-1} = \frac{v}{c_v T^2}\begin{bmatrix} \bar{e}_5 & u_1\bar{e}_3 & u_2\bar{e}_3 & u_3\bar{e}_3 & -\bar{e}_2 \\ & \bar{c}_1 & u_{12} & u_{31} & -u_1 \\ & & \bar{c}_2 & u_{23} & -u_2 \\ & \text{symm} & & \bar{c}_3 & -u_3 \\ & & & & 1 \end{bmatrix}. \tag{A.16}$$

The advective Jacobians with respect to U, $A_i = F_{i,U}$, are given by

$$A_1 = \begin{bmatrix} 0 & 1 & 0 & 0 & 0 \\ a^2 - u_1^2 - \bar{e}_1\bar{\gamma} & -u_1(\bar{\gamma} - 2) & -u_2\bar{\gamma} & -u_3\bar{\gamma} & \bar{\gamma} \\ -u_{12} & u_2 & u_1 & 0 & 0 \\ -u_{31} & u_3 & 0 & u_1 & 0 \\ -u_1(e_1 + \bar{e}_1\bar{\gamma} - a^2) & e_1 - u_1^2\bar{\gamma} & -u_{12}\bar{\gamma} & -u_{31}\bar{\gamma} & u_1(\bar{\gamma} + 1) \end{bmatrix}, \tag{A.17}$$

$$A_2 = \begin{bmatrix} 0 & 0 & 1 & 0 & 0 \\ u_{12} & u_2 & u_1 & 0 & 0 \\ a^2 - u_2^2 - \bar{e}_1\bar{\gamma} & -u_1\bar{\gamma} & -u_2(\bar{\gamma} - 2) & u_3\bar{\gamma} & \bar{\gamma} \\ -u_{23} & 0 & u_3 & u_2 & 0 \\ -u_2(e_1 + \bar{e}_1\bar{\gamma} - a^2) & -u_{12}\bar{\gamma} & e_1 - u_2^2\bar{\gamma} & -u_{23}\bar{\gamma} & u_2(\bar{\gamma} + 1) \end{bmatrix}, \tag{A.18}$$

$$A_3 = \begin{bmatrix} 0 & 0 & 0 & 1 & 0 \\ -u_{31} & u_3 & 0 & u_1 & 0 \\ -u_{23} & 0 & u_3 & u_2 & 0 \\ a^2 - u_3^2 - \bar{e}_1\bar{\gamma} & -u_1\bar{\gamma} & -u_2\bar{\gamma} & -u_3(\bar{\gamma}-2) & \bar{\gamma} \\ -u_3(e_1 + \bar{e}_1\bar{\gamma} - a^2) & -u_{31}\bar{\gamma} & -u_{23}\bar{\gamma} & e_1 - u_3^2\bar{\gamma} & u_3(\bar{\gamma}+1) \end{bmatrix}. \tag{A.19}$$

The advective Jacobian matrices with respect to V, $\tilde{A}_i = F_{i,V} = \tilde{A}_i\tilde{A}_0$, are given by

$$\tilde{A}_1 = \frac{\beta_T T}{v^2}\begin{bmatrix} u_1 & c_1 & u_{12} & u_{31} & u_1 e_3 \\ & u_1\left(u_1^2 + 3\dfrac{v}{\beta_T}\right) & u_2 c_1 & u_3 c_1 & e_1\dfrac{v}{\rho_T} + u_1^2 e_4 \\ & & u_1 c_2 & u_{123} & u_{12} e_4 \\ & \text{symm} & & u_1 c_3 & u_{31} e_4 \\ & & & & u_1\left(e_5 + 2e_1\dfrac{v}{\beta_T}\right) \end{bmatrix}, \tag{A.20}$$

$$\tilde{A}_2 = \frac{\beta_T T}{v^2}\begin{bmatrix} u_2 & u_{12} & c_2 & u_{23} & u_2 e_3 \\ & u_2 c_1 & u_1 c_2 & u_{123} & u_{12} e_4 \\ & & u_2\left(u_2^2 + 3\dfrac{v}{\beta_T}\right) & u_3 c_2 & e_1\dfrac{v}{\beta_T} + u_2^2 e_4 \\ & \text{symm} & & u_2 c_3 & u_{23} e_4 \\ & & & & u_2\left(e5 + 2e_1\dfrac{v}{\beta_T}\right) \end{bmatrix}, \tag{A.21}$$

$$\tilde{A}_3 = \frac{\beta_T T}{v^2}\begin{bmatrix} u_3 & u_{31} & u_{23} & c_3 & u_3 e_3 \\ & u_3 c_1 & u_{123} & u_1 c_3 & u_{31} e_4 \\ & & u_3 c_2 & u_2 c_3 & u_{23} e_4 \\ & \text{symm} & & u_3\left(u_3^2 + 3\dfrac{v}{\beta_T}\right) & e_1\dfrac{v}{\beta_T} + u_3^2 e_4 \\ & & & & u_3\left(e_5 + 2e_1\dfrac{v}{\beta_T}\right) \end{bmatrix}. \tag{A.22}$$

The right-hand side coefficient matrices $\tilde{K}_{ij}$, where $\tilde{K}_{ij}V_{,j} = F_i^h$ are given by

$$\hat{K}_{ij} = K\delta_{ij}, \tag{A.23}$$

where

$$K = \begin{bmatrix} 0 & 0 & 0 & 0 & 0 \\ & 0 & 0 & 0 & 0 \\ & & 0 & 0 & 0 \\ & \text{symm} & & 0 & 0 \\ & & & & \dfrac{\kappa n}{m} T^2 \end{bmatrix}. \tag{A.24}$$

The source vector in terms of the V variables is given as

$$\boldsymbol{F} = \frac{T}{v}\left\{\begin{array}{c} 0 \\ \dfrac{\varepsilon}{m} E_1 V_5 + \dfrac{\varepsilon}{m\mu_{n0}T_0}\dfrac{V_2}{V_5} \\ \dfrac{\varepsilon}{m} E_2 V_5 + \dfrac{\varepsilon}{m\mu_{n0}T_0}\dfrac{V_3}{V_5} \\ \dfrac{\varepsilon}{m} E_3 V_5 + \dfrac{\varepsilon}{m\mu_{n0}T_0}\dfrac{V_4}{V_5} \\ -\dfrac{\varepsilon}{m}(E_1V_2 + E_2V_3 + E_3V_4) - \dfrac{\left(c_v - \dfrac{V_2^2+V_3^2+V_4^2}{2V_5} + \dfrac{3}{2}k_b\dfrac{T_0}{m}V_5\right)}{\left[\dfrac{3}{2}\dfrac{\mu_{n0}}{\varepsilon v_S^2}\dfrac{k_bT_0}{1-V_5T_0} - \dfrac{m\mu_{n0}T_0V_5}{2\varepsilon}\right]} \end{array}\right\}, \tag{A.25}$$

where T/v is expressed in terms of V variables as given in (A.5). The source coefficient-matrix, $\tilde{C}$ (where $\tilde{C}V = -F$), is not uniquely defined. One possible definition, which leads to a symmetric matrix, is

$$\tilde{C} = -\frac{T}{v}\begin{bmatrix} 0 & 0 & 0 & 0 & 0 \\ 0 & \dfrac{\varepsilon}{m\mu_{n0}T_0V_5} & 0 & 0 & \dfrac{\varepsilon E_1}{m} \\ 0 & 0 & \dfrac{\varepsilon}{m\mu_{n0}T_0V_5} & 0 & \dfrac{\varepsilon E_2}{m} \\ 0 & 0 & 0 & \dfrac{\varepsilon}{m\mu_{n0}T_0V_5} & \dfrac{\varepsilon E_3}{m} \\ 0 & \dfrac{\varepsilon E_1}{m} & \dfrac{\varepsilon E_2}{m} & \dfrac{\varepsilon E_3}{m} & \bar{\omega} \end{bmatrix}, \tag{A.26}$$

where

$$\bar{\omega} = -2\frac{\varepsilon}{m}\frac{(E_1V_2 + E_2V_3 + E_3V_4)}{V_5} - \frac{\left(c_v - \dfrac{V_2^2+V_3^2+V_4^2}{2V_5} + \dfrac{3}{2}k_b\dfrac{T_0}{m}V_5\right)}{\left[\dfrac{3}{2}\dfrac{\mu_{n0}}{\varepsilon v_S^2}\dfrac{k_bT_0}{1-V_5T_0} - \dfrac{m\mu_{n0}T_0V_5}{2\varepsilon}\right]V_5}. \tag{A.27}$$

Acknowledgment

This research was sponsored by DARPA through contract no. DAA100391-C-0043. The authors would like to thank Drs. Datong Chen, Ke Chih Wu, Zhiping Yu and Zdenek Johan for helpful discussions, and Dr. Farzin Shakib for providing us with the initial code for Euler and Navier–Stokes analysis. The equipment support provided by Digital Equipment Corporation to Professor K.H. Law is appreciated.

Notation

ε electronic charge
κ conductivity per unit volume
μ specific chemical potential
μ_{n0} low field electronic mobility
θ dielectric permittivity
ψ electrostatic potential
ψ_b built-in potential
ψ_{appl} applied bias
ψ^h finite element approximation of potential
$\bar{\psi}^h$ finite element weighting function for Poisson problem
τ_p momentum relaxation time
τ_w energy relaxation time
Ω spatial domain
Ω_n^e element spatial domain at the nth time slab
γ ratio of specific heats
υ^h discontinuity capturing factor
v specific volume
τ least squares matrix
Γ boundary of spatial domain
Γ_g boundary on which essential boundary conditions are prescribed
Γ_h boundary on which natural boundary conditions are prescribed
$\tilde{A}_i$ Euler Jacobian matrix with respect to conservative variables in direction i
$\tilde{A}_i$ Euler Jacobian matrix with respect to entropy variables in direction i
$\tilde{A}_0$ Riemannian metric tensor
B_n boundary of nth space time slab
$\tilde{C}$ source coefficient matrix
c_v specific heat at constant volume
c_p specific heat at constant pressure
E electric field vector
E_i electric field in direction i
e_{tot} electron total energy per unit mass
e_{int} electron internal energy per unit mass
F source vector
F_i Euler flux vector in direction i
F_i^h heat flux vector in direction i
g prescribed boundary condition vector for HD equations
g_p prescribed boundary condition for Poisson problem
$\mathcal{H}$ entropy function
h_i prescribed natural boundary condition in direction i for Poisson problem
I_n time interval
$\tilde{K}$ diffusivity matrix with respect to conservative variables
$\tilde{K}$ diffusivity matrix with respect to entropy variables

k_b Boltzmann constant
L reference length
$M^{(i)}$ consistent tangent matrix at ith iterative step for HD system
m electron mass
N_D^+ concentration of ionized donor
N_A^- concentration of ionized acceptor
$N_A^{(n)}$ finite element spatial shape function of node A for the nth time slab
n concentration of electrons
n_d doping concentration
n_i intrinsic concentration of electrons
n_{np} number of nodal points
n_{dof} number of degrees of freedom for HD system
p_e, $\boldsymbol{p}$ electron momentum density vector
p_h hole momentum density vector
p concentration of holes
P electron pressure per unit mass
t time
Q_n space time slab at time level n
Q_n^e element space time slab at time level n
q_e, $\boldsymbol{q}$ electron heat flux vector
q_h hole heat flux vector
q_i heat flux in direction i
$\boldsymbol{R}^i$ residual vector at ith iterative step for HD system
R specific gas constant
s thermodynamic entropy
T_e, T temperature of electrons
T_h temperature of holes
T_0 temperature of the lattice
$\boldsymbol{U}$ conservative variables vector
u_e, $\boldsymbol{u}$ electron velocity vector
u_h hole velocity vector
u_i velocity in direction i
v_s saturation velocity
$\boldsymbol{V}$ entropy variable vector
$\boldsymbol{V}^h$ finite element trial solution vector
V_t reference voltage
$\boldsymbol{v}_A$ vector of nodal unknowns at node A for HD system
$\boldsymbol{W}^h$ weighting function vector for hydrodynamic equations
w_e, w electron energy density
w_h hole energy density
w_A weighting function vector at node A for HD system
$[\,]_{col}$ collision terms
$(\,)^*$ nondimensional quantity
$(\,)_0$ reference value

References

[1] M.R. Pinto, Comprehensive semiconductor device simulation for silicon ULSI, Dept. of Elec. Engrg., Ph.D. Thesis, Stanford University, 1990.
[2] D. Chen et al., Elimination of spurious velocity overshoot using a new energy transport model, unpublished.
[3] G. Baccarani and M.R. Wordeman, An investigation of steady-state velocity overshoot in silicon, Solid-State Electron. 28 (1985) 407–416.
[4] M. Rudan and F. Odeh, Multi-dimensional discretization scheme for the hydrodynamic model of semiconductor devices, COMPEL 5 (1986) 149–183.
[5] M. Rudan, F. Odeh and J. White, Numerical solution of the hydrodynamic model for a one-dimensional device, COMPEL 6 (1987) 151–170.
[6] C.L. Gardner, J.W. Jerome and D.J. Rose, Numerical methods for the hydrodynamic device model: Subsonic flow, IEEE Trans. Comput. Aided Design 8 (1989) 501–507.
[7] E. Fatemi, J.W. Jerome and S. Osher, Solution of the hydrodynamic device model using high-order nonoscillatory shock capturing algorithms, IEEE Trans. Comput. Aided Design 10 (1991) 232–244.
[8] T.J.R. Hughes, Recent progress in the development and understanding of SUPG methods with special reference to the compressible Euler and Navier–Stokes equations, Internat. J. Numer. Methods Engrg. 7 (1987) 1261–1275.
[9] T.J.R. Hughes, M. Mallet and A. Mizukami, A new finite element formulation for computational fluid dynamics: II. Beyond SUPG, Comput. Methods Appl. Mech. Engrg. 54 (1986) 341–355.
[10] F. Shakib, Finite element analysis of the compressible Euler and Navier–Stokes equations, Dept. of Mech. Engrg., Ph.D. Thesis, Stanford University, 1988.
[11] Z. Johan, Data parallel finite element techniques for large-scale computational fluid dynamics, Dept. of Mech. Engrg., Ph.D. Thesis, Stanford University, 1992.
[12] K. Blotekjaer, Transport equations for electrons in two-valley semiconductors, IEEE Trans. Electron. Devices 17 (1970) 38–47.
[13] S. Selberherr, An Analysis and Simulation of Semiconductor Devices (Springer, New York, 1984).
[14] A. Harten, On the symmetric form of systems of conservation laws with entropy, J. Comput. Phys. 49 (1983) 151–164.
[15] T.J.R. Hughes, L.P. Franca and M. Mallet, A new finite element formulation for computational fluid dynamics: I. Symmetric forms of the compressible Euler and Navier–Stokes equations and the second law of thermodynamics, Comput. Methods Appl. Mech. Engrg. 54 (1986) 223–234.
[16] F. Chalot, T.J.R. Hughes and F. Shakib, Symmetrization of conservation laws with entropy for high-temperature hypersonic computations, Comput. Systems Engrg. 1 (1990) 494–521.
[17] A. Mizukami and T.J.R. Hughes, A Petrov–Galerkin finite element method for convection-dominated flows: an accurate upwinding technique for satisfying the maximum principle, Comput. Methods Appl. Mech. Engrg. 50 (1985) 181–193.
[18] C. Johnson, Streamline diffusion methods for problems in fluids, in: R.H. Gallagher et al., eds, Finite Elements in Fluids, Vol. VI (Wiley, London, 1986) 251–261.
[19] T.J.R. Hughes and M. Mallet, A new finite element formulation for computational fluid dynamics: IV. A discontinuity-capturing operator for multidimensional advective-diffusive systems, Comput. Methods Appl. Mech. Engrg. 58 (1986) 329–336.
[20] A.C. Galeão and E.G. Dutra Do Carmo, A consistent approximate upwind Petrov–Galerkin method for convection-dominated problems, Comput. Methods Appl. Mech. Engrg. 68 (1988) 83–95.
[21] T.J.R. Hughes, L.P. Franca and G.M. Hulbert, A new finite element formulation for computational fluid dynamics: VIII. The Galerkin/least-squares method for advective-diffusive equations, Comput. Methods Appl. Mech. Engrg. 73 (1989) 173–189.
[22] T.J.R. Hughes and M. Mallet, A new finite element formulation for computational fluid dynamics: III. The generalized streamline operator for multidimensional advective-diffusive systems, Comput. Methods Appl. Mech. Engrg. 58 (1986) 305–328.
[23] T.J.R. Hughes, The Finite Element Method: Linear Static and Dynamic Finite Element Analysis (Prentice Hall, Englewood Cliffs, NJ, 1987).
[24] R.L. Lee, P.M. Gresho and R.L. Sani, Smoothing techniques for certain primitive variable solutions of the Navier–Stokes equations, Internat. J. Numer. Methods Engrg. 14 (1979) 1785–1804.
[25] C. Johnson, U. Nävert and J. Pitkäranta, Finite element methods for linear hyperbolic problems, Comput. Methods Appl. Mech. Engrg. 45 (1984) 285–312.